J Nanopart Res (2017) 19: 289
DOI 10.1007/s11051-017-3970-z

RESEARCH PAPER

Efficient photodegradation of methylthioninium chloride dye in aqueous using barium tungstate nanoparticles

Saad M. AlShehri · Jahangeer Ahmed · Tansir Ahamad · Basheer M. Almaswari · Aslam Khan

Received: 30 March 2017 / Accepted: 13 July 2017 / Published online: 16 August 2017

Abstract $BaWO_4$ nanoparticles were successfully used as the photocatalysts in the degradation of methylthioninium chloride (MTC) dye at different pH levels of aqueous solution. Pure phase of barium tungstate ($BaWO_4$) nanoparticles was synthesized by modified molten salt process at 500 °C for 6 h. Structural and morphological characterizations of $BaWO_4$ nanoparticles (average particle size of ~40 nm) were studied in details using powder x-ray diffraction (XRD), FTIR, Raman, energy-dispersive, electron microscopic, and x-ray photoelectron spectroscopy (XPS) techniques. Direct band gap energy of $BaWO_4$ nanoparticles was found to be ~3.06 eV from the UV–visible absorption spectroscopy followed by Tauc's model. Photocatalytic properties of the nanoparticles were also investigated systematically for the degradation of MTC dye solution in various mediums. $BaWO_4$ nanoparticles claim the significant enhancement of the photocatalytic degradation of aqueous MTC dye to non-hazardous inorganic constitutes under alkaline, neutral, and acidic mediums.

Keywords Nanoparticles · XPS · Degradation · Photocatalysis · Environmental effects

S. M. AlShehri (✉) · J. Ahmed (✉) · T. Ahamad · B. M. Almaswari
Department of Chemistry, College of Science, King Saud University, Riyadh 11451, Saudi Arabia
e-mail: alshehri@ksu.edu.sa
e-mail: jahmed@ksu.edu.sa

A. Khan
King Abdullah Institute for Nanotechnology, King Saud University, Riyadh 11451, Saudi Arabia

Introduction

Wastewater treatment is an important concern to control the water pollution and health risks, worldwide, by the destruction of organic pollutants like organic dyes (e.g., methylthioninium chloride, rhodamine B, methyl orange) from water. One slice of the most hazardous substances in wastewater is organic dyes because these are widely used in many industrial applications including plastics, cosmetics, drugs, textiles, paper, leather, etc. Numerous methods like solvent extraction (El-Ashtoukhy and Fouad 2015; Lee et al. 2000), adsorption (Alqadami et al. 2016; Naushad et al. 2016; Zhu et al. 2012), chemical precipitation, and coagulation (Bowie and Bond 1977) were employed in the removal of hazardous substances from water. The biggest challenge to the researchers is to develop the efficient and cost-effective procedures for wastewater treatment. Photocatalysis is an effective, eco-friendly, economical, and simple process for the purification of wastewater by the removal of organic and inorganic pollutants from aqueous. Several semiconducting nanostructured materials including TiO_2 (Das et al. 2012; Huang et al. 2013; Liu et al. 2011; Qamar et al. 2009; Seftel et al. 2015; Zhang et al. 2017), MWCNT/TiO_2 (Zouzelka et al. 2016), GO/TiO_2 (Jin et al. 2014; Radich et al. 2014; Yang et al. 2016b), heteroatom-doped graphene–TiO_2 (Tian et al. 2017), Fe_2O_3/TiO_2 (Ahmed et al. 2013), GO/TiO_2/Au (Yang et al. 2016a), Ag/ZnO (Arab Chamjangali et al. 2015), ZnO (Shen et al. 2008), CdS (Ahmed et al. 2016), GO/CdS (Wang et al. 2012), ZnO/CdS (Khanchandani et al. 2012), CdS/SiO_2, SnO_2 (Kim

et al. 2016), Mn_3O_4 (Larbi et al. 2016), $NiMn_2O_4$ (Larbi et al. 2016), WO_3 (Visa et al. 2015), Pt/WO_3 (Fujii et al. 2015), TiO_2/WO_3 (Anandan et al. 2014), $WO_3/ZnWO_4$ (Keereeta et al. 2015), Co-$BiVO_4$ (Zhou et al. 2010), $BaMoO_4$ (Bazarganipour 2016), etc. were extensively used as the photocatalysts in the degradation of aqueous organic dyes. $BaWO_4$ is a semiconducting material and has a band gap in the range from 3.2 to 5.6 eV (Khademolhoseini and Ali Zarkar 2016; Mohamed Jaffer Sadiq and Samson Nesaraj 2015; Pontes et al. 2003; Tyagi et al. 2010; Vidya et al. 2013). Recently, $BaWO_4$ nanoparticles were used as the photocatalysts in the removal of organic pollutants (e.g., rhodamine B and methyl orange) from water (Khademolhoseini and Ali Zarkar 2016; Mohamed Jaffer Sadiq and Samson Nesaraj 2015). Manganese oxide pyrolusites were used as the photocatalysts for the degradation of methylene blue at various pH levels (acidic and basic mediums) of the solution (Kuan and Chan 2012). In this paper, we present that the $BaWO_4$ nanoparticles were used as the photocatalysts in the degradation of organic pollutants (e.g., methylthioninium chloride dye) from water at different pH levels. Methylthioninium chloride (MTC) is a basic aniline dye (general formula: $C_{16}H_{18}ClN_3S$) which is also known as methylene blue (MB) dye. MTC also leads to a number of health complications including affected central nervous system, breast cancer, and gastrointestinal disturbances in human being (Kida et al. 2003; Piscatelli et al. 2009; Vutskits et al. 2008).

$BaWO_4$ nanostructured materials have also shown the potential in various applications including low-temperature cofired ceramics (LTCC) (Vidya et al. 2013), nitrogen oxide sensors (Tamaki et al. 1995), non-enzymatic glucose biosensors (Mani et al. 2016), optical (Ge et al. 2005; Nikl et al. 2000; Tyagi et al. 2010; Vidya et al. 2013), photoluminescence (Anicete-Santos et al. 2011; Cavalcante et al. 2009a; Cavalcante et al. 2009b; Yin et al. 2010; Zhang et al. 2013), light-emitting diodes (Yang et al. 2009), microwave dielectrics (Wang and Bian 2014), etc. Metal oxide nanostructured materials (with different shape and size) have been synthesized from the various chemical methods including reverse micelle (Ahmed et al. 2012; Kwan et al. 2001; Shi et al. 2002; Shi et al. 2003), solvothermal (Zhang et al. 2006), hydrothermal (Cavalcante et al. 2009a; Zhang et al. 2013), surfactant-assisted hydrothermal (Liu and Chu 2005), sonochemical (Khademolhoseini and Ali Zarkar 2016; Thongtem et al. 2008), coprecipitation (Mohamed Jaffer Sadiq and Samson Nesaraj 2015; Phuruangrat et al. 2012), microwave heating (Shen et al. 2011), combustion (Vidya et al. 2013), etc. Microcrystals of $BaWO_4$ materials were also prepared by the molten flux method using alkali metal nitrates with 12-fold in excess at 400–500 °C for 12 h (Afanasiev 2007). Pure phase of $BaWO_4$ nanoparticles in tetragonal unit cell structure was synthesized from the modified molten salt method using sodium nitrate and potassium nitrate as the reaction mediums at 500 °C for 6 h. X-ray diffraction (XRD), FTIR, Raman, XPS, EDS, and electron microscopic studies were carried out for structural and morphological characterizations of $BaWO_4$ nanoparticles. Optical and photocatalytic properties of $BaWO_4$ nanoparticles were investigated in details. UV–vis spectrophotometer and electrospray ionization mass spectrometer (ESI-MS) techniques were employed to study the photocatalytic degradation of MTC dye over the surface of $BaWO_4$ nanoparticles.

Materials and methods

$Ba(NO_3)_2$ (BDH, 98%), $Na_2WO_4{\cdot}2H_2O$ (BDH, 96%), $NaNO_3$ (Alfa Aesar, 98+%), and KNO_3 (Alfa Aesar, 99%) reagents were used in the synthesis of $BaWO_4$ nanoparticles by the molten salt method. The molten salts were taken with the molar ratio of 1:1:40:40 of $Ba(NO_3)_2/Na_2WO_4{\cdot}2H_2O/NaNO_3/KNO_3$ and mixed together in an agate mortar pestle for 30 min to make the homogenous mixture. Subsequently, the resulting homogenous mixture of the molten salts was transferred to the covered ceramic crucible and kept at 500 °C for 6 h in temperature-controlled furnace with the heating and cooling rate of 10 °C per minute. The white-colored product was washed several times by de-ionized water and then dried at 50 °C in an oven. Previously, micron-sized particles of $BaWO_4$ were prepared by the molten flux method using $BaCl_2$, alkali metal tungstate, and either $NaNO_3$ or KNO_3 in the molar ratio of 1:1:12 in the temperature range from 400 to 600 °C for 12 h (Afanasiev 2007).

The white-colored nanopowders were characterized by powder XRD on an x-ray diffractometer (Rigaku MiniFlex) using Ni-filtered Cu-Kα radiation. XRD data was recorded with a step size and a scan speed of 0.02° and 1 s, respectively. FTIR studies were investigated on a Bruker TENSOR 27 spectrometer in the range of wave number from 400 to 4000 cm^{-1}. Raman spectroscopic

measurements were done on a Renishaw instrument with an Ar laser source of 488 nm. Field emission scanning electron microscopic (FESEM) studies were done on a JEOL JSM-7600F electron microscope operated at 5 kV. High-resolution transmission electron microscopic (HRTEM) analyses were accomplished on a JEOL JSM-2100F electron microscope (Tokyo, Japan) operated at 200 kV. X-ray photoelectron spectroscopy (XPS) was acquired on a Kratos Axis Ultra DLD (Chestnut Ridge, NY) to confirm the chemical composition of the nanoparticles. BET surface area of the $BaWO_4$ nanoparticles was measured on a V-Sorb 2800 Porosimetry analyzer (Gold APP Instruments, China). The absorption spectroscopic studies of the $BaWO_4$ nanoparticles were performed on a UV–vis spectrophotometer (Shimadzu, UV-1650) with a single-beam diode array spectrometer in a wavelength range from 200 to 800 nm using a slit width of 1 nm. Deuterium (D) and tungsten (W) lamps were used to afford the illumination across the UV and visible electromagnetic spectrum. Absorption spectrum was typically collected from 1 mL of sample dispersion using a standard quartz cuvette with the path of 1 cm. The photocatalytic activities of $BaWO_4$ nanoparticles were investigated against the organic dye (MTC as a pollutant) in water under the irradiation of sunlight at different pH levels. The degradation studies of MTC dye solutions were carried out at room temperature at pH 4, 7, and 10 using a UV–vis spectrophotometer at λ_{max} of 662.5 nm with the photocatalytic reaction intervals. All the samples were taken in sample cuvette with high transparency to measure the absorption spectra of photodegradation of dye solution. Note that the photocatalytic experiments were repeated twice to check the reproducibility of the present results. The degradation rate constants of MTC dye using $BaWO_4$ nanoparticles as the photocatalysts were calculated using the following equation (i.e., first-order reaction kinetic): $\ln(C/C_0) = -kt$, where C, C_0, k, and t are the concentrations of MTC dye after time (t), initial concentration of MTC dye, rate of degradation constant, and time, respectively. An electrospray ionization mass spectrometer (ESI-MS, Agilent Triple Quadrupole) was used to investigate the quantitative analysis of the photodegraded MTC dye. The ESI-MS spectral data was obtained with 34 scans (0.3 s each) at the fragmented voltage of 100 V.

Results and discussions

Figure 1a shows the XRD pattern of $BaWO_4$ nanoparticles obtained from the molten salt method at 500 °C. XRD pattern clearly shows the formation of pure $BaWO_4$ phase with zero impurity phases. All the diffraction peaks [(101), (112), (004), (202), (211), (204), (220), (116), (215), (132), (224), and (008)] are perfectly indexed on the basis of tetragonal unit cell structure of $BaWO_4$ (JCPDS 72-0746). Figure 1b shows the FTIR spectrum of $BaWO_4$ nanoparticles in the range of wave number from 400 to 4000 cm^{-1}. The bands at ~1380 and ~3414 cm^{-1} correspond to the bending vibration and stretching vibration of $–CH_2$ and –OH groups, respectively. A strong band at ~824 corresponds to the antisymmetric stretching vibration of W–O in $[WO_4]^{2-}$ tetrahedron as also reported previously (Mohamed Jaffer Sadiq and Samson Nesaraj 2015) that confirms the formation of barium tungstate. Figure 1c represents the Raman spectrum of $BaWO_4$ nanoparticles. Raman bands of $BaWO_4$ nanoparticles at ~926 and ~334 cm^{-1} belong to the non-degenerate symmetric stretching vibration, and the bands at ~797 and 832 cm^{-1} resemble to degenerate asymmetric stretching vibration of W–O in $[WO_4]^{2-}$ tetrahedron while the Raman mode at 274 cm^{-1} could be assigned on the basis of symmetric stretching vibration of BaO_6 octahedron. Raman modes of tetragonal $BaWO_4$ nanoparticles were also reported elsewhere and the present work also supports to the previous reports (Hardcastle and Wachs 1995; M Zawawi et al. 2013).

X-ray photoelectron spectroscopy (XPS) measurements were carried out to obtain the oxidation state of cations and the surface chemical composition of $BaWO_4$. The XPS spectrum of $BaWO_4$ (Fig. 3a) reveals the presence of Ba, W, and O elements in the nanoparticles with no impurities. The high-resolution Ba 3d spectrum is shown in Fig. 2b that consists of two spectral lines at 780.30 and 795.69 eV, corresponding to the Ba $3d_{5/2}$ and Ba $3d_{3/2}$ lines, respectively (Shi et al. 2003). Figure 2c shows the high-resolution W 4f spectrum that also consists of two more spectral lines at 35.42 and 37.6 eV, which correspond to the W $4f_{7/2}$ and W $4f_{5/2}$ lines, respectively (He et al. 2015). The O 1s spectrum is shown in Fig. 2d. The component at 531.07 eV was assigned to the oxygen in $BaWO_4$.

FESEM studies of $BaWO_4$ nanoparticles are shown in Fig. 3. FESEM micrographs show the formation of uniform and monodispersed nanoparticles of $BaWO_4$. A careful visualization of size and shape analysis of

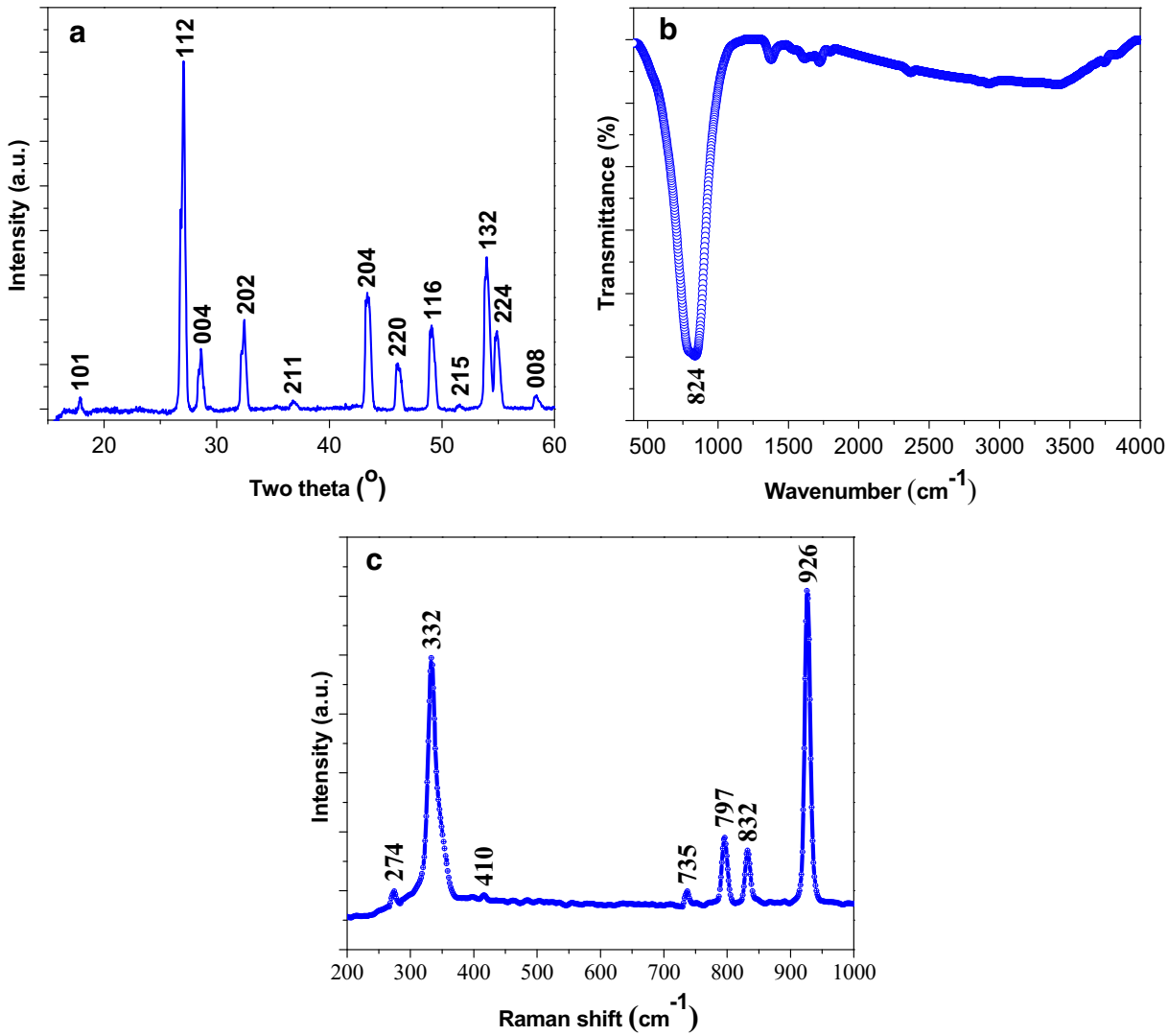

Fig. 1 **a** XRD pattern, **b** FTIR, and **c** Raman spectra of $BaWO_4$ nanoparticles

$BaWO_4$ nanoparticles is shown in Fig. 3b, c. Excerpt of FESEM micrograph shows that the nanoparticles are spherical in shape with uniform particle size distributions and the average particle size was found to be ~40 nm. The significance of uniform and monodispersed nanoparticles could be ascribed to the uniform physicochemical properties of distinct particles in the dispersion medium. Therefore, monodispersed nanoparticles with uniform size could be more effective in their respective applications like sensing, energy conversion and conservation, adsorption, photocatalytic wastewater treatments, etc. Previously, Afanasiev (2007) reported the molten salt synthesis of microcrystalline polyhedral-shaped barium tungstate particles with an average size of ~10 μm. The major differences between the previous and present procedures are the nature of molten salts and the molar ratio of precursor materials and molten salts used in the chemical reactions. In this procedure, molten salts function as the solvent like water and excess of molten salts plays the fundamental role in terms of transferring of the sufficient amount of energy to the precursor materials to control the size of the final product materials in nanometric region. This is noteworthy that the molten salt procedure is one of the most favorable, simple, eco-friendly, and less expensive method to synthesize the pure phase nanostructured materials with uniform particles size. Figure 3b shows the energy-dispersive x-ray spectroscopic (EDS) studies (equipped

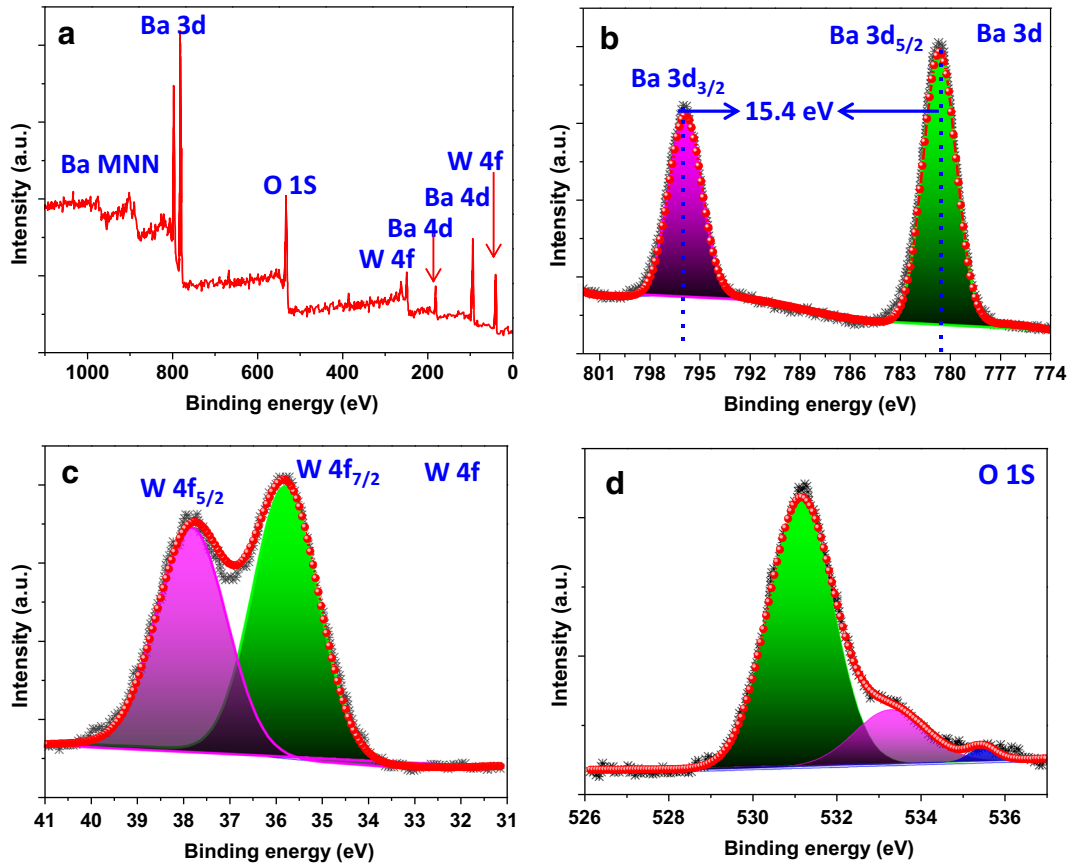

Fig. 2 XPS spectra of **a** $BaWO_4$, **b** Ba 3d, **c** W4f, and **d** O1s

with FESEM machine) of $BaWO_4$ nanoparticles for the elemental analysis. The atomic weight percent of the elements in the nanoparticles was found to be 10.30 and 9.64% of Ba and W, respectively, which matches with the initial loaded composition. TEM studies support the FESEM results and confirm the shape and size of $BaWO_4$ nanoparticles. Figure 4a shows the formation of spherical-shaped nanoparticles with the particle size

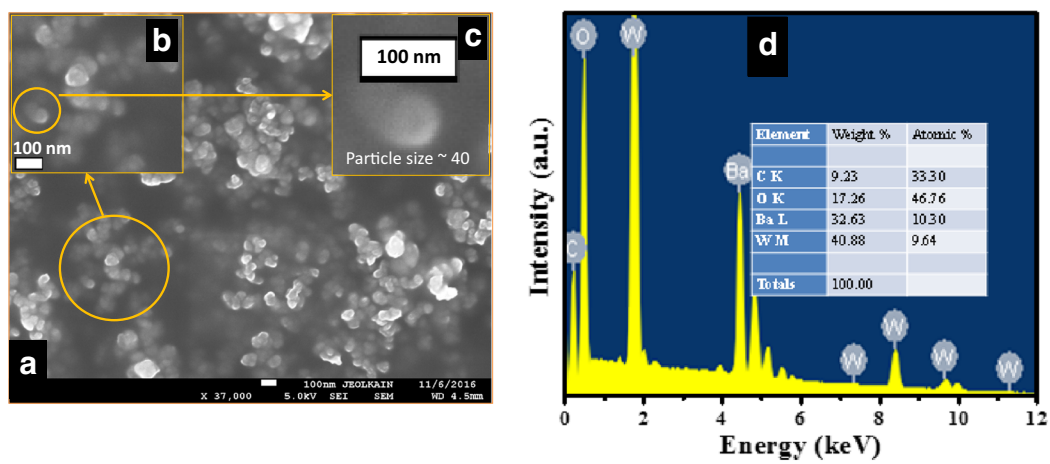

Fig. 3 **a** FESEM image of $BaWO_4$ nanoparticles. **b**, **c** Excerpt of FESEM data for careful particle size analysis of $BaWO_4$ nanoparticles. **d** Energy-dispersive x-ray spectroscopic studies of $BaWO_4$ nanoparticles

range from 30 to 40 nm as also observed in FESEM studies. High-resolution transmission electron microscopic (HRTEM) studies showed that the $BaWO_4$ nanoparticles are very crystalline in nature (Fig. 4b). The lattice d-spacing value of $BaWO_4$ nanoparticles was found to be ~3.37 Å from HRTEM studies, which is a good agreement with highly intense plane (112) of tetragonal crystal structure of $BaWO_4$ nanoparticles. Specific BET (Brunauer–Emmett–Teller) surface area (S_{BET}) of $BaWO_4$ nanoparticles was studied using the N_2 adsorption–desorption isotherm. S_{BET} of $BaWO_4$ nanoparticles was found to be ~4.46 m^2/g that is larger (more than two times) than the earlier reported S_{BET} of $BaWO_4$ nanoparticles (~2.30 m^2/g) (M Zawawi et al. 2013). The pore size distribution (1.75 nm) of the resulting $BaWO_4$ nanoparticles was found to be smaller than that of the previously reported pore size distribution (1.92 nm) of the $BaWO_4$ nanoparticles (M Zawawi et al. 2013).

Optical properties of $BaWO_4$ nanoparticles were also investigated at room temperature from the UV–vis absorption spectroscopic studies. Optical absorption spectroscopy is one of the strong techniques to examine the optical properties of nanocrystalline materials. The optical absorbance spectrum for $BaWO_4$ nanoparticles was recorded in the region of ultraviolet A (i.e., UV region from 315 to 400 nm) with the peak value of 344 nm (Fig. 5a). UV–vis absorption spectroscopy works with some factors in order to find the bands in ultraviolet and visible reasons, i.e., (1) dispersed light due to scattering counted as absorbed light by the UV–vis spectrophotometer and (2) optical absorption due to electronic transitions of the sample. The fundamental absorption studies (visible and near UV spectral range) led to the generation of electron-hole pair as a result of optical excitation of electrons from the valence band to the conduction band. The minimum quantum energy sufficient to electron excitation from the valence band to the conduction band is equal to the band gap of the semiconductor. The optical band gap energy of $BaWO_4$ nanoparticles was experimentally calculated through the UV–vis absorption spectrum studies using Tauc's model (Tauc 1968). Figure 5b shows a plot of band gap energy (i.e., photon energy) versus $(\alpha h\nu)^2$ for $BaWO_4$ nanoparticles, where α, h, and ν are represented as the absorbance (obtained from absorption spectrum), Planck's constant, and frequency of incident beam, respectively. The optical band gap energy, extrapolation of the straight line, of $BaWO_4$ nanoparticles was found to be ~3.06 eV, which is lower than that of other reports (Khademolhoseini and Ali Zarkar 2016; Mohamed Jaffer Sadiq and Samson Nesaraj 2015; Pontes et al. 2003; Tyagi et al. 2010; Vidya et al. 2013). Lower value of band gap energy could be possible due to the

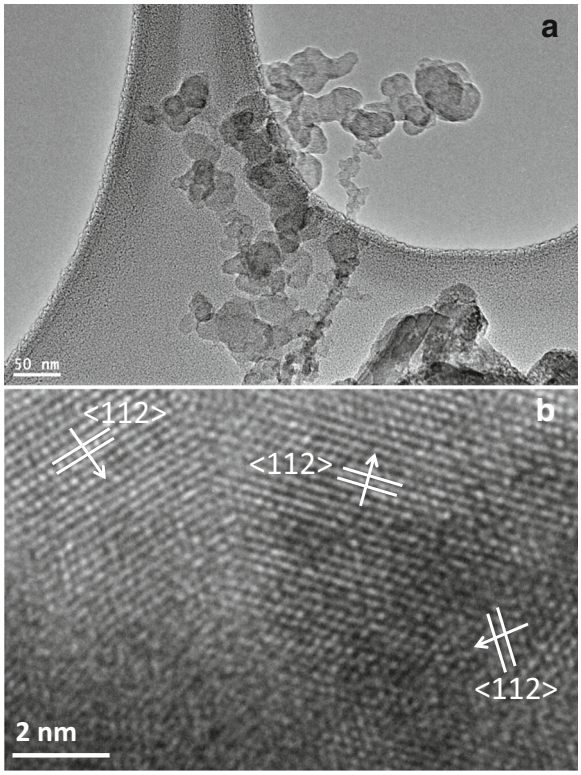

Fig. 4 **a** TEM and **b** HRTEM micrographs of $BaWO_4$ nanoparticles

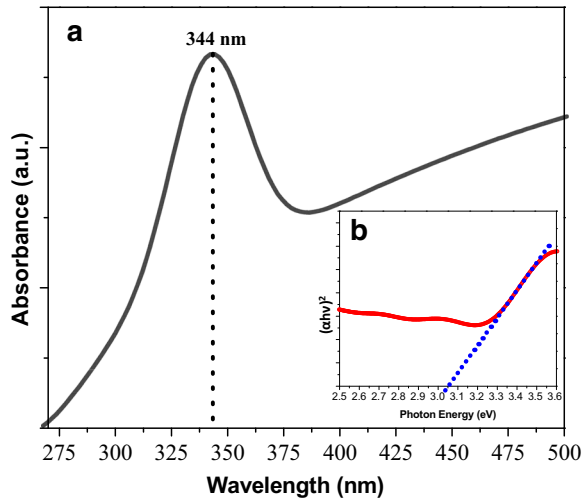

Fig. 5 **a** Absorption spectrum and **b** plot of $(\alpha h\nu)^2$ vs photon energy (eV) for the evaluation of direct band gap of $BaWO_4$ nanoparticles

following key parameters: changes in symmetry of lattice, electronic states, electronegativity of tungsten ions, deviation in bonds (i.e., O–W–O bonds), distortion of the $[WO_4]^{2-}$ tetrahedrons, oxygen vacancy, etc. (Vidya et al. 2013). The band gap energy is the energy difference between the valance and the conduction band of the materials. $BaWO_4$ nanoparticles retain the wide band gap in the visible region that could be an appropriate material in the transparent conducting oxide films for the solar cells and photocatalytic applications.

The photocatalytic efficiency of $BaWO_4$ nanoparticles was examined in the degradation of methylthioninium chloride (MTC) dye under the sunlight irradiation at different pH values, i.e., 4, 7, and 10. Figure 6 represents the photocatalytic mechanism for the degradation of organic dye to inorganic constituents with $BaWO_4$ nanoparticles. Photocatalytic degradation of MTC dye on the surface of nanoparticles could be described in terms of the generation of oxidizing agents, i.e., hydroxyl free radicals (OH·). Photocatalytic activity of $BaWO_4$ nanoparticles arises due to the recombination of electron (e^-)–hole (h^+) pairs. The electrons (e^-) are excited from the valence band to the conduction band, and the holes (h^+) are formed on the valence band of $BaWO_4$ nanoparticles after the irradiation of solar light. Note that the photonic energy is larger than the band gap energy of $BaWO_4$ nanoparticles (3.06 eV), which is estimated experimentally from the UV–vis absorption studies as discussed above. The e^- and h^+ pairs were produced the superoxide radical anion ($O_2^{-}\cdot$) and hydroxyl radicals ($\dot{O}H\cdot$), respectively, in aqueous medium at the atmospheric condition (i.e., in presence of oxygen). The hydroxyl radicals (OH·) attack on the MTC dye molecule to give the oxidized products. The photocatalytic reactions could be summarized in the following steps as given below (note that BWO resembles as $BaWO_4$ nanoparticles in the following steps):

$$BWO + h\upsilon \rightarrow BWO(e^- + h^+)$$

$$BWO\ (h^+) + H_2O \rightarrow BWO + OH^{\bullet} + H^+$$

$$BWO(h^+) + HO^- \rightarrow BWO + OH^{\bullet}$$

In the conduction band, the electrons (e^-) of BWO reduce the molecular O_2 to the protonated form of superoxide ($O_2^{\bullet-}$):

$$BWO + O_2 + e^- \rightarrow BWO + O_2^{\bullet-}$$

$$O_2^{\bullet-} + H^+ \rightarrow HO_2^{\bullet}$$

Formation of hydrogen peroxide followed by further reduction of molecular O_2

$$2HO_2^{\bullet-} \rightarrow H_2O_2 + O_2$$

$$H_2O_2 + e^- \rightarrow OH^- + OH^{\bullet}$$

The degradation of the adsorbed complexes (i.e., MTC dye) via direct oxidation process on the surface of BWO photocatalysts gives the oxidized products as shown below:

$$OH\cdot + MTC \rightarrow MTC\cdot + H_2O$$

$$MTC + h^+ \rightarrow MTC^+\cdot (\textit{degraded products}, \text{i.e.}, CO_2)$$

The resulting oxidized products could be appeared in the form of H_2O, CO_2, NO_3^-, and SO_4^{2-} after the complete degradation of MTC dye over the surface of photocatalysts, as also reported previously (Houas et al. 2001).

The photocatalytic degradation of MTC dye in aqueous at pH 7 is shown in Fig. 7. The characteristic peak of organic dye (i.e., MTC) was detected at the absorbance of 662.5 nm in the UV–vis absorption spectra. We observed that the absorption band intensities were diminished with time (t) in the presence of $BaWO_4$ nanoparticles under the sunlight irradiations (Fig. 7a). Reduction in the absorption band intensities of aqueous MTC dye solution indicates the degradation of dye by the irradiation of light on the surface of $BaWO_4$ nanoparticles. Figure 7b shows the linear plot (i.e., kinetic plot) of degradation efficiencies of MTC dye with time versus $\ln(C_0/C_t)$, which provides the kinetic behavior of the photocatalytic reactions. The rate constant of reaction was observed from the slope of curve fitting line. The photocatalytic degradation of MTC dye over the surface of $BaWO_4$ nanoparticles follows the first-order decay kinetics, and the rate constant (k) was estimated from the kinetic equation (i.e., $\ln(C_0/C_t) = kt$, where C_0, C_t, t, and k are the initial concentrations of MTC, concentration of MTC at various time intervals, time, and rate constant, respectively). The kinetic linear plots of

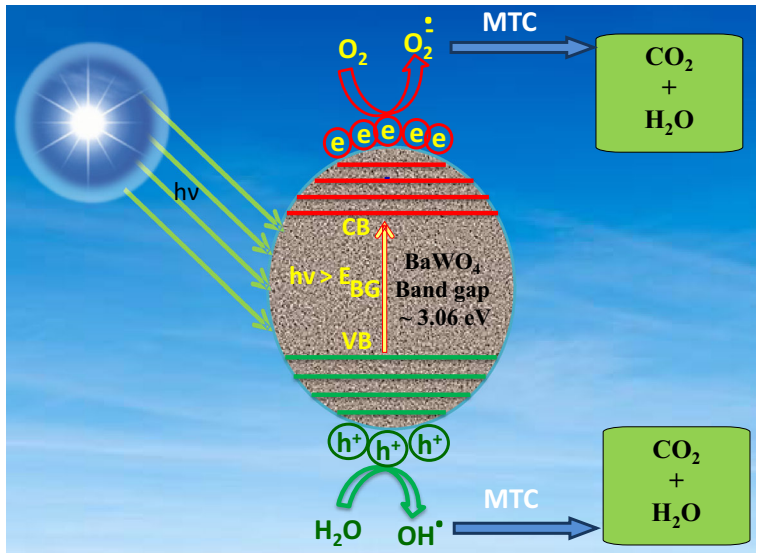

Fig. 6 Proposed mechanism of photocatalytic degradation of MTC dye on the surface of $BaWO_4$ nanoparticles

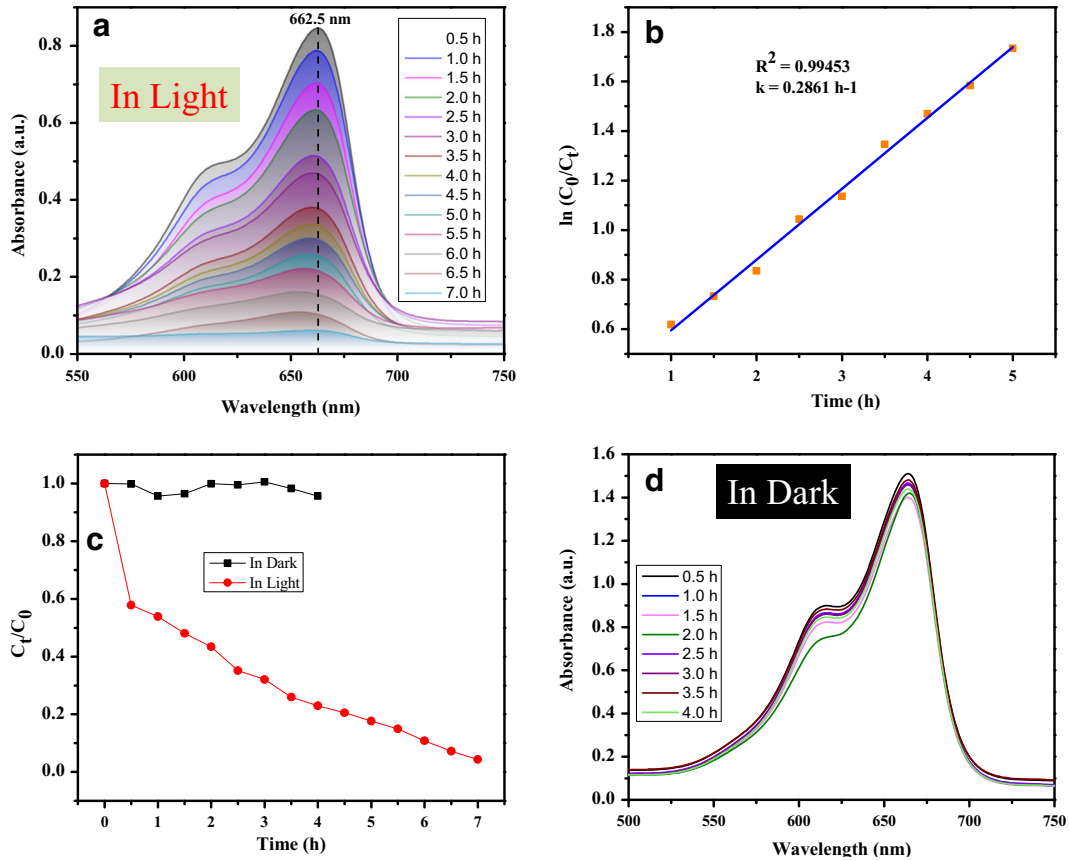

Fig. 7 **a** Absorption spectra of photocatalytic degradation of MTC dye under sunlight irradiations over $BaWO_4$ nanoparticles at pH 7. **b** Linear plot ln(C_0/C_t) vs time for pseudo-first-order reaction kinetics of photodegradation of MTC dye with $BaWO_4$ nanoparticles. **c** Photocatalytic degradation of MTC dye in presence or absence of sunlight at pH 7. **d** UV–vis absorption spectra of MTC dye in the dark with $BaWO_4$ nanoparticles at pH 7

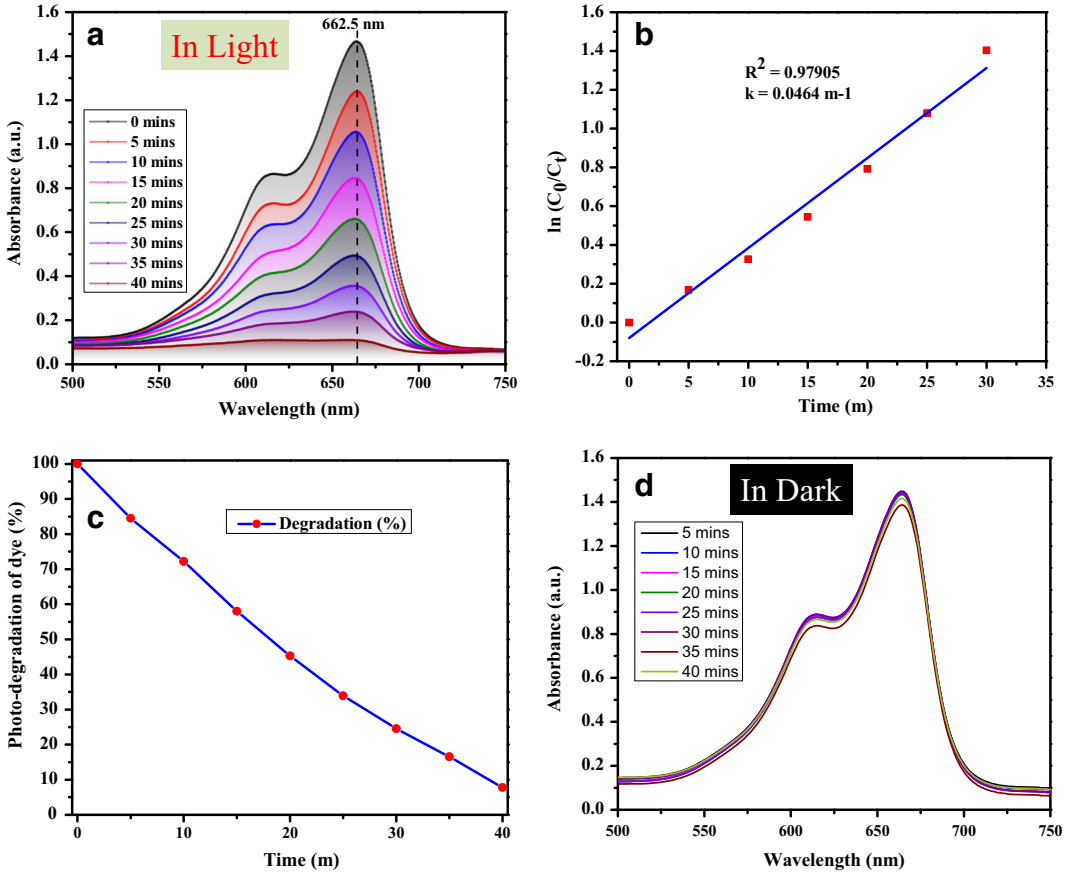

Fig. 8 **a** Absorption spectra of photodegradation of organic dye (MTC) with $BaWO_4$ nanoparticles in alkaline medium (i.e., pH = 10) in the presence of sunlight. **b** Linear plot of $\ln(C_0/C_t)$ vs time for pseudo-first-order reaction kinetics. **c** Photocatalytic degradation of MTC dye under sunlight irradiation with $BaWO_4$ nanoparticles. **d** UV–vis absorption spectra of dye with $BaWO_4$ nanoparticles at pH 10 in the dark

$\ln(C_0/C_t)$ vs "t" suggested the pseudo-first-order reaction with the rate constants and R^2 value of (slope) of 0.2861 h^{-1} and ~0.9945, respectively (Fig. 7b). This is noteworthy that the maximal value of absorption wavelength (i.e., 662.5 nm) was not changed during the degradation of organic dye over the surface of $BaWO_4$ photocatalysts. Figure 7c shows the variation of the photocatalytic activity of $BaWO_4$ nanoparticles at the maximal value with time (t) of irradiation of sunlight. The rate of photocatalytic degradation was obtained from the equation containing primary concentration and the concentration after the irradiation time (t) of the dye solution, i.e., $(C_t/C_0) \times 100\%$. $BaWO_4$ nanoparticles degraded the MTC dye solution up to 97% in the presence of sunlight for 7 h. Figure 7d shows the absorption spectra of MTC dye in the dark with $BaWO_4$ nanoparticles at pH 7. It is notable that no catalytic degradation of MTC dye occurred in the presence of $BaWO_4$ nanoparticles in the dark. The stability of photocatalysts is also an important concern for the industrialization. Therefore, $BaWO_4$ nanoparticles were also optimized for the recyclable process in the photodegradation of MTC dye. These nanoparticles as the photocatalysts show recyclable efficiency with excellent activity for the degradation of MTC dye solution under the irradiation of sunlight. Note that the nanoparticles have been washed from the distilled water followed by drying at 50 °C after the completion of each cycle. The photocatalytic stability of $BaWO_4$ nanoparticles was observed using the several consecutive cycles to evaluate the photocatalytic reactivity of the nanoparticles after the exposure to UV irradiations. It is clearly observed that the $BaWO_4$ photocatalysts hold high reactivity (i.e., up to ~70%) and stability after the six consecutive cycles against the UV irradiations in neutral medium.

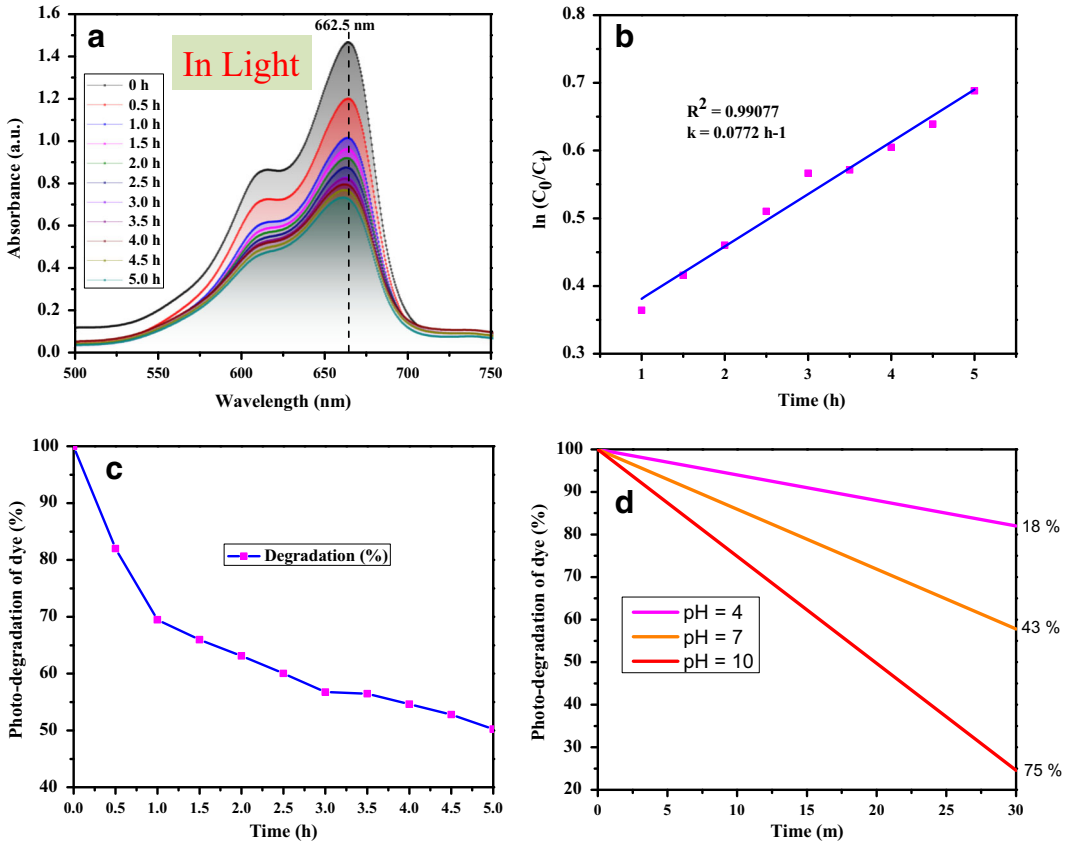

Fig. 9 **a** UV–vis absorption spectra of degradation of dye on to the surface of $BaWO_4$ nanoparticles at pH 4 in light. **b** $\ln(C_0/C_t)$ vs time (t) linear plot for reaction kinetics. **c** Photocatalytic degradation of MTC dye with $BaWO_4$ nanoparticles at pH 4. **d** Relative photocatalytic studies in different mediums for the degradation of organic dye for 30 min

Furthermore, the catalytic degradation of MTC dye solution using the $BaWO_4$ photocatalysts has also been investigated in alkaline medium (i.e., pH = 10). Figure 8a shows the absorption spectra of MTC dye solution at the wavelength of 662.5 nm. Absorption studies reveal that the photocatalytic degradation process of the organic pollutant (i.e., MTC dye) into inorganic substances was conceded to be very fast in alkaline medium compared to the neutral medium without alteration of the absorption wavelength of MTC dye (662.5 nm) with the time (t). The kinetic linear plot of $\ln(C_0/C_t)$ vs time has been shown in Fig. 8b. Pseudo-first-order kinetic reaction was clearly observed experientially with the rate constants and R^2 values of 0.0464 min^{-1} and ~0.97905, respectively. Figure 8c, d shows the photocatalytic activity of $BaWO_4$ nanoparticles for the degradation of MTC dye in alkaline medium (at pH = 10) in the presence of solar light irradiation. This is noteworthy that the photodegradation process of MTC dye in alkaline medium was found to be faster (~93% degraded within 40 min) compared to the neural medium under the irradiation of solar light. Earlier, nanocrystalline $BaWO_4$ particles were used as the photocatalysts for the degradation of organic dye (rhodamine B and methyl orange) in the presence of light. $BaWO_4$ nanoparticles degraded the methyl orange ~70% within 70 min and rhodamine B ~90% within 180 min in water under the light irradiations (Khademolhoseini and Ali Zarkar 2016; Mohamed Jaffer Sadiq and Samson Nesaraj 2015). The rate of photodegradation process of organic dye over the surface of nanoparticles depends on the formation of hydroxyl radicals. In alkaline medium, more numbers of hydroxyl radicals (attacking species) are formed, which lead to the faster rate of reaction. The catalytic degradation of MTC dye on to the surface of nanoparticles was also inspected in the dark at pH 10, and we found that no degradation of organic dye (MTC) was detected with time (Fig. 8d). $BaWO_4$ nanoparticles are recyclable, stable, and efficient photocatalysts for the photodegradation of organic dye in alkaline medium.

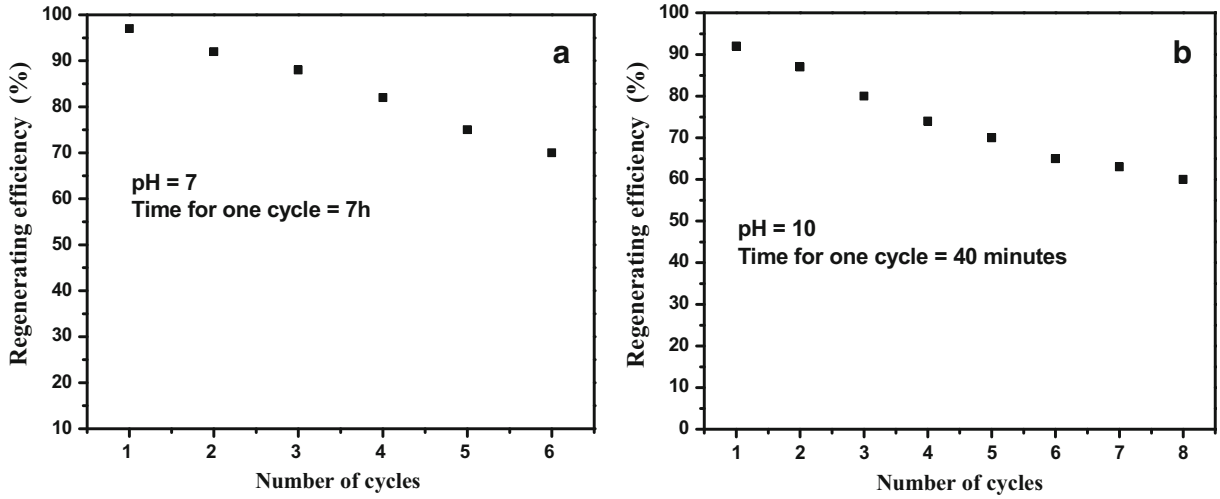

Fig. 10 Photocatalytic regeneration efficiency of $BaWO_4$ nanoparticles against the UV irradiations at **a** pH = 7 and **b** pH = 10

$BaWO_4$ photocatalysts claim the reactivity up to 60% after eight successive cycles against the UV irradiations in alkaline medium (i.e., pH = 10). Before using for each cycle, the nanoparticles were washed appropriately with distilled water and dried properly at 50 °C in an oven.

Additionally, the photocatalytic degradation of organic pollutant (i.e., MTC dye) was also investigated in acidic medium (i.e., pH = 4). The absorption spectra of MTC dye under sunlight irradiations at 662.5 nm are shown in Fig. 9a. This study exposed that the photocatalytic degradation process of MTC dye with the time was found to be very slow in acidic medium as compared to neutral and alkaline mediums. The kinetic plot ($\ln(C_0/C_t)$ vs time) showed pseudo-first-order reaction with the rate constants and R^2 values of 0.0772 h^{-1} and ~0.99077, respectively (Fig. 9b). Figure 9c shows the photocatalytic activity of $BaWO_4$ nanoparticles for the degradation of dye at pH 4 in the presence of sunlight.

The comparative photocatalytic studies of the degradation of organic dye for 30 min in different aqueous mediums (acidic, neutral, and alkaline mediums) are shown in Fig. 9d. The results show that the dye has been degraded 75, 43, and 18% within 30 min at pH of 10, 7, and 4, respectively. Therefore, the present results reveal that the photocatalytic degradations of MTC dye solution on to the surface of nanoparticles significantly depend on the nature of aqueous solution of organic dye. The rate of photocatalytic degradation of dye with time was found to be higher in alkaline medium compared to the neutral and acidic mediums, which also supports the previous work reported on the photodegradation of MB with manganese oxide pyrolusites (Kuan and Chan 2012). The reason behind the enhancement of photocatalytic degradation in alkaline medium is the formation of hydroxyl radicals (i.e., highly reactive species) in larger amount compared to acidic or neutral medium during the irradiation of sunlight by the

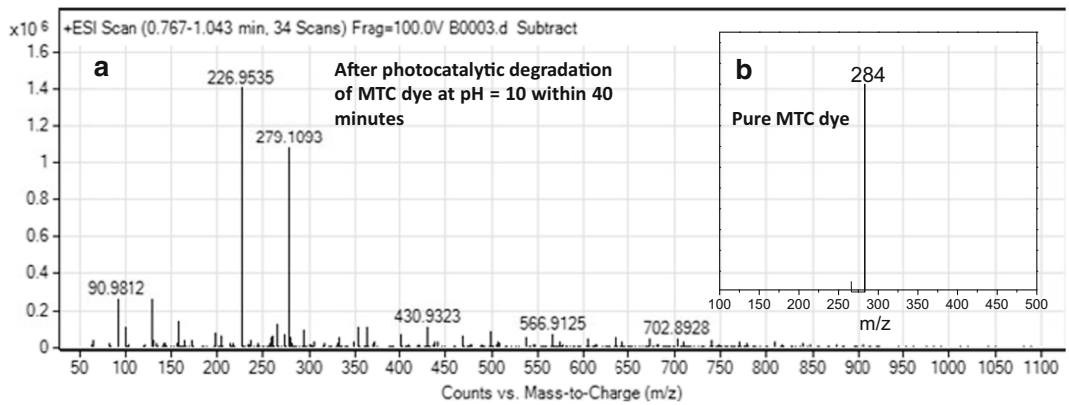

Fig. 11 **a** ESI-MS spectrum of MTC dye after photocatalytic degradation at pH 10. **b** ESI-MS spectrum of pure MTC dye

dissociation of H_2O_2 molecules. Therefore, the rate of photocatalytic degradation of organic dye in alkaline medium over the surface of $BaWO_4$ nanoparticles was found to be very high than the other mediums (acidic or neutral).

$BaWO_4$ nanoparticles are recyclable, stable, and efficient photocatalysts for the photodegradation of organic dye solutions in alkaline medium and neutral medium. The photocatalytic stability of $BaWO_4$ nanoparticles was observed using the several consecutive cycles to evaluate the photocatalytic reactivity of the nanoparticles after the exposure to UV irradiations at pH 7 and 10 (Fig. 10). It is clearly observed that the $BaWO_4$ photocatalysts hold high reactivity (i.e., up to ~70%) and stability after the six consecutive cycles against the UV irradiations at pH of 7 (Fig. 10a) while $BaWO_4$ photocatalysts claim the reactivity up to 60% after eight successive cycles against the UV irradiations in alkaline medium (i.e., pH = 10) as also shown in Fig. 10b. Before using for each cycle, the nanoparticles were washed appropriately with distilled water and dried properly at 50 °C in an oven.

ESI-MS studies confirm the photodegradation of dye molecules at pH 10 within 40 min of irradiation, and no peak of pure MTC dye was observed (i.e., at *m*/*z* of 284) in Fig. 11a. The ESI-MS signals at *m*/*z* of 279.1093 ($C_{13}H_{15}N_2O_3S^+$), 226.9535 ($C_{13}H_{11}N_2S^+$), and 90.9812 ($C_6H_6N^+$) could be indexed on the basis of the fragmentations of the dye molecules by the attack of hydroxyl and superoxide free radicals. The most active bonds of MTC dye are C–N and C–S, which were broken by the attack of free radicals. Thereafter, the resulting oxidized molecules could be converted into inorganic constituents like CO_2, NH_3, H_2O, etc. The present results were also supported by the previous reports on degradation of MB dye (Amini et al. 2014; Oliveira et al. 2015). Figure 11b shows ESI-MS spectral studies of the pure MTC dye where the signal at *m*/*z* of 284 was clearly observed. Note that the single at *m*/*z* of 284 is missing in Fig. 11a, which indicates that the organic dye is almost degraded and the resulting signals correspond to the fragmentation of the dye molecules.

Conclusions

$BaWO_4$ nanoparticles were synthesized from the molten salt method at 500 °C for 6 h. The optical properties of $BaWO_4$ nanoparticles were studied using UV–visible absorption spectroscopy, and the direct band gap energy of $BaWO_4$ nanoparticles was found to be ~3.06 eV. $BaWO_4$ nanoparticles were used as the photocatalysts for the degradation of MTC dye at various pH levels with time. $BaWO_4$ nanoparticles show enhanced photodegradation of MTC dye solution in alkaline medium compared to the neutral and acidic mediums. $BaWO_4$ nanoparticles are stable and significantly recyclable photocatalysts for the degradation of organic dye in neutral and alkaline mediums. This study could be useful in the industrial wastewater treatment plants by the deprivation of hazardous dyes into inorganic substances like H_2O, CO_2, etc.

Acknowledgements The authors extend their sincere appreciation to the Deanship of Scientific Research at King Saud University for funding this Research Group (RG-1435-007).

Compliance with ethical standards

Conflict of interest The authors declare that they have no conflict of interest.

References

Afanasiev P (2007) Molten salt synthesis of barium molybdate and tungstate microcrystals. Mater Lett 61:4622–4626. doi:10.1016/j.matlet.2007.02.061

Ahmed J, Blakely CK, Bruno SR, Poltavets VV (2012) Synthesis of MSnO3 (M = Ba, Sr) nanoparticles by reverse micelle method and particle size distribution analysis by whole powder pattern modeling. Mater Res Bull 47:2282–2287. doi:10.1016/j.materresbull.2012.05.044

Ahmed MA, El-Katori EE, Gharni ZH (2013) Photocatalytic degradation of methylene blue dye using Fe2O3/TiO2 nanoparticles prepared by sol–gel method. J Alloys Compd 553: 19–29. doi:10.1016/j.jallcom.2012.10.038

Ahmed B, Kumar S, Kumar S, Ojha AK (2016) Shape induced (spherical, sheets and rods) optical and magnetic properties of CdS nanostructures with enhanced photocatalytic activity for photodegradation of methylene blue dye under ultra-violet irradiation. J Alloys Compd 679:324–334. doi:10.1016/j.jallcom.2016.03.295

Alqadami AA, Naushad M, Abdalla MA, Khan MR, Alothman ZA (2016) Adsorptive removal of toxic dye using Fe3O4–TSC nanocomposite: equilibrium, kinetic, and thermodynamic studies. J Chem Eng Data 61:3806–3813. doi:10.1021/acs.jced.6b00446

Amini M, Pourbadiei B, Ruberu TPA, Woo LK (2014) Catalytic activity of MnOx/WO3 nanoparticles: synthesis, structure characterization and oxidative degradation of methylene blue. New J Chem 38:1250–1255. doi:10.1039/C3NJ01563G

Anandan S, Sivasankar T, Lana-Villarreal T (2014) Synthesis of TiO2/WO3 nanoparticles via sonochemical approach for the photocatalytic degradation of methylene blue under visible light illumination. Ultrason Sonochem 21:1964–1968. doi:10.1016/j.ultsonch.2014.02.015

Anicete-Santos M, Picon FC, Alves CN, Pizani PS, Varela JA, Longo E (2011) The role of short-range disorder in BaWO4 crystals in the intense green photoluminescence. J Phys Chem C 115:12180–12186. doi:10.1021/jp2009622

Arab Chamjangali M, Bagherian G, Javid A, Boroumand S, Farzaneh N (2015) Synthesis of Ag–ZnO with multiple rods (multipods) morphology and its application in the simultaneous photo-catalytic degradation of methyl orange and methylene blue. Spectrochim Acta A Mol Biomol Spectrosc 150:230–237. doi:10.1016/j.saa.2015.05.067

Bazarganipour M (2016) Synthesis and characterization of BaMoO4 nanostructures prepared via a simple sonochemical method and their degradation ability of methylene blue. Ceram Int 42:12617–12622. doi:10.1016/j.ceramint.2016.04.151

Bowie JE, Bond MT (1977) Chemical precipitation-coagulation for organic color removal from groundwaters1 JAWRA J Am Water Resour Assoc 13:1269–1280 doi:10.1111/j.1752-1688.1977.tb02096.x

Cavalcante LS, Sczancoski JC, Espinosa JWM, Varela JA, Pizani PS, Longo E (2009a) Photoluminescent behavior of BaWO4 powders processed in microwave-hydrothermal. J Alloys Compd 474:195–200. doi:10.1016/j.jallcom.2008.06.049

Cavalcante LS, Sczancoski JC, Lima LF, Espinosa JWM, Pizani PS, Varela JA, Longo E (2009b) Synthesis, characterization, anisotropic growth and photoluminescence of BaWO4. Cryst Growth Des 9:1002–1012. doi:10.1021/cg800817x

Das D, Shivhare A, Saha S, Ganguli AK (2012) Room temperature synthesis of mesoporous TiO2 nanostructures with high photocatalytic efficiency. Mater Res Bull 47:3780–3785. doi:10.1016/j.materresbull.2012.06.021

El-Ashtoukhy ESZ, Fouad YO (2015) Liquid–liquid extraction of methylene blue dye from aqueous solutions using sodium dodecylbenzenesulfonate as an extractant. Alex Eng J 54:77–81. doi:10.1016/j.aej.2014.11.007

Fujii A, Meng Z, Yogi C, Hashishin T, Sanada T, Kojima K (2015) Preparation of Pt-loaded WO3 with different types of morphology and photocatalytic degradation of methylene blue. Surf Coat Technol 271:251–258. doi:10.1016/j.surfcoat.2014.11.070

Ge W et al (2005) The thermal and optical properties of BaWO4 single crystal. J Cryst Growth 276:208–214. doi:10.1016/j.jcrysgro.2004.11.385

Hardcastle FD, Wachs IE (1995) Determination of the molecular structures of tungstates by Raman spectroscopy. J Raman Spectrosc 26:397–405. doi:10.1002/jrs.1250260603

He G et al (2015) One pot synthesis of nickel foam supported self-assembly of NiWO4 and CoWO4 nanostructures that act as high performance electrochemical capacitor electrodes. J Mater Chem A 3:14272–14278. doi:10.1039/C5TA01598G

Houas A, Lachheb H, Ksibi M, Elaloui E, Guillard C, Herrmann J-M (2001) Photocatalytic degradation pathway of methylene blue in water. Appl Catal B Environ 31:145–157. doi:10.1016/S0926-3373(00)00276-9

Huang H, Leung DYC, Kwong PCW, Xiong J, Zhang L (2013) Enhanced photocatalytic degradation of methylene blue under vacuum ultraviolet irradiation. Catal Today 201:189–194. doi:10.1016/j.cattod.2012.06.022

Jin C, Cui X, Tian H, Wang X, Sun C, Zheng W (2014) Photo-less catalysis of TiO2-reduced graphene oxides. Chem Phys Lett 608:229–234. doi:10.1016/j.cplett.2014.06.007

Keereeta Y, Thongtem S, Thongtem T (2015) Enhanced photocatalytic degradation of methylene blue by WO3/ZnWO4 composites synthesized by a combination of microwave-solvothermal method and incipient wetness procedure. Powder Technol 284:85–94. doi:10.1016/j.powtec.2015.06.046

Khademolhoseini S, Ali Zarkar S (2016) Preparation and characterization of barium tungstate nanoparticles via a new simple surfactant-free route. J Mater Sci Mater Electron 27:9605–9609. doi:10.1007/s10854-016-5016-1

Khanchandani S, Kundu S, Patra A, Ganguli AK (2012) Shell thickness dependent photocatalytic properties of ZnO/CdS core–shell nanorods. J Phys Chem C 116:23653–23662. doi:10.1021/jp3083419

Kida M, Kobayashi K, Saigenji K (2003) Routine chromoendoscopy for gastrointestinal diseases: indications revised. Endoscopy 35:590–596. doi:10.1055/s-2003-40228

Kim SP, Choi MY, Choi HC (2016) Photocatalytic activity of SnO2 nanoparticles in methylene blue degradation. Mater Res Bull 74:85–89. doi:10.1016/j.materresbull.2015.10.024

Kuan W-H, Chan Y-C (2012) pH-dependent mechanisms of methylene blue reacting with tunneled manganese oxide pyrolusite. J Hazard Mater 239–240:152–159. doi:10.1016/j.jhazmat.2012.08.051

Kwan S, Kim F, Akana J, Yang P (2001) Synthesis and assembly of BaWO4 nanorods. Chem Commun. 447-448 doi: 10.1039/B100005P

Larbi T, Ben said L, Ben daly A, Ouni B, Labidi A, Amlouk M (2016) Ethanol sensing properties and photocatalytic degradation of methylene blue by Mn3O4, NiMn2O4 and alloys of Ni-manganates thin films. J Alloys Compd 686:168–175. doi:10.1016/j.jallcom.2016.06.001

Lee DW, Hong WH, Hwang KY (2000) Removal of an organic dye from water using a predispersed solvent extraction. Sep Sci Technol 35:1951–1962. doi:10.1081/SS-100100629

Liu Y, Chu Y (2005) Surfactant-assisted synthesis of single crystal BaWO4 octahedral microparticles. Mater Chem Phys 92:59–63. doi:10.1016/j.matchemphys.2004.12.030

Liu B, Khare A, Aydil ES (2011) TiO2–B/anatase core–shell heterojunction nanowires for photocatalysis. ACS Appl Mater Interfaces 3:4444–4450. doi:10.1021/am201123u

M Zawawi SM, Yahya R, Hassan A, HNME M, Daud MN (2013) Structural and optical characterization of metal tungstates (MWO4; M=Ni, Ba, Bi) synthesized by a sucrose-templated method. Chem Cent J 7:80. doi:10.1186/1752-153x-7-80

Mani S, Vediyappan V, Chen S-M, Madhu R, Pitchaimani V, Chang J-Y, Liu S-B (2016) Hydrothermal synthesis of NiWO4 crystals for high performance non-enzymatic glucose biosensors. Sci Rep 6:24128. doi:10.1038/srep24128

Mohamed Jaffer Sadiq M, Samson Nesaraj A (2015) Soft chemical synthesis and characterization of BaWO4 nanoparticles for photocatalytic removal of Rhodamine B present in water sample. J Nanostruct Chem 5:45–54. doi:10.1007/s40097-014-0133-y

Naushad M, Abdullah Alothman Z, Rabiul Awual M, Alfadul SM, Ahamad T (2016) Adsorption of rose Bengal dye from aqueous solution by amberlite Ira-938 resin: kinetics, isotherms, and thermodynamic studies. Desalin Water Treat 57:13527–13533. doi:10.1080/19443994.2015.1060169

Nikl M et al (2000) Excitonic emission of scheelite tungstates AWO4 (A=Pb, Ca, Ba, Sr). J Lumin 87–89:1136–1139. doi:10.1016/S0022-2313(99)00569-4

Oliveira HS, Oliveira LCA, Pereira MC, Ardisson JD, Souza PP, Patricio PO, Moura FCC (2015) Nanostructured vanadium-

doped iron oxide: catalytic oxidation of methylene blue dye. New J Chem 39:3051–3058 doi:10.1039/C4NJ02063D

Phuruangrat A, Thongtem T, Thongtem S (2012) Precipitate synthesis of BaMoO4 and BaWO4 nanoparticles at room temperature and their photoluminescence properties. Superlattice Microst 52:78–83. doi:10.1016/j.spmi.2012.04.016

Piscatelli N, Crawford S, Larkin A, Robert Q, Layeequr Rahman R (2009) Complications of methylene blue dye infiltration for sentinel lymph node biopsy in breast cancer. Cancer Res 69:4140. doi:10.1158/0008-5472.sabcs-4140

Pontes FM et al (2003) Preparation, structural and optical characterization of BaWO4 and PbWO4 thin films prepared by a chemical route. J Eur Ceram Soc 23:3001–3007. doi:10.1016/S0955-2219(03)00099-2

Qamar M, Kim SJ, Ganguli AK (2009) TiO 2-based nanotubes modified with nickel: synthesis, properties, and improved photocatalytic activity. Nanotechnology 20:455703

Radich JG, Krenselewski AL, Zhu J, Kamat PV (2014) Is graphene a stable platform for photocatalysis? Mineralization of reduced graphene oxide with UV-irradiated TiO2 nanoparticles. Chem Mater 26:4662–4668. doi:10.1021/cm5026552

Seftel EM, Niarchos M, Mitropoulos C, Mertens M, Vansant EF, Cool P (2015) Photocatalytic removal of phenol and methylene-blue in aqueous media using TiO2@LDH clay nanocomposites. Catal Today 252:120–127. doi:10.1016/j.cattod.2014.10.030

Shen W, Li Z, Wang H, Liu Y, Guo Q, Zhang Y (2008) Photocatalytic degradation for methylene blue using zinc oxide prepared by codeposition and sol–gel methods. J Hazard Mater 152:172–175. doi:10.1016/j.jhazmat.2007.06.082

Shen Y, Li W, Li T (2011) Microwave-assisted synthesis of BaWO4 nanoparticles and its photoluminescence properties. Mater Lett 65:2956–2958. doi:10.1016/j.matlet.2011.06.033

Shi H, Qi L, Ma J, Cheng H (2002) Synthesis of single crystal BaWO4 nanowires in catanionic reverse micelles. Chem Commun 1704–1705 doi: 10.1039/B204995C

Shi H, Qi L, Ma J, Cheng H (2003) Polymer-directed synthesis of penniform BaWO4 nanostructures in reverse micelles. J Am Chem Soc 125:3450–3451. doi:10.1021/ja029958f

Tamaki J, Fujii T, Fujimori K, Miura N, Yamazoe N (1995) Application of metal tungstate-carbonate composite to nitrogen oxides sensor operative at elevated temperature. Sensors Actuators B Chem 25:396–399. doi:10.1016/0925-4005(95)85089-9

Tauc J (1968) Optical properties and electronic structure of amorphous Ge and Si. Mater Res Bull 3:37–46. doi:10.1016/0025-5408(68)90023-8

Thongtem T, Phuruangrat A, Thongtem S (2008) Characterization of MeWO4 (Me = Ba, Sr and Ca) nanocrystallines prepared by sonochemical method. Appl Surf Sci 254:7581–7585. doi:10.1016/j.apsusc.2008.01.092

Tian H, Shen K, Hu X, Qiao L, Zheng W (2017) N, S co-doped graphene quantum dots-graphene-TiO2 nanotubes composite with enhanced photocatalytic activity. J Alloys Compd 691:369–377. doi:10.1016/j.jallcom.2016.08.261

Tyagi M, Singh SG, Chauhan AK, Gadkari SC (2010) First principles calculation of optical properties of BaWO4: a study by full potential method. Phys B Condens Matter 405:4530–4535. doi:10.1016/j.physb.2010.08.032

Vidya S, Solomon S, Thomas JK (2013) Synthesis, characterization, and low temperature sintering of nanostructured BaWO4 for optical and LTCC applications. Adv Condens Matter Phys. 2013:11 doi: 10.1155/2013/409620.

Visa M, Bogatu C, Duta A (2015) Tungsten oxide—fly ash oxide composites in adsorption and photocatalysis. J Hazard Mater 289:244–256. doi:10.1016/j.jhazmat.2015.01.053

Vutskits MDPDL et al (2008) Adverse effects of methylene blue on the central nervous system. Anesthesiology 108:684–692. doi:10.1097/ALN.0b013e3181684be4

Wang Z, Bian JJ (2014) Low temperature sintering and microwave dielectric properties of Ba3(PO4)2–BaWO4 composite ceramics. Ceram Int 40:8507–8511. doi:10.1016/j.ceramint.2014.01.062

Wang X, Tian H, Yang Y, Wang H, Wang S, Zheng W, Liu Y (2012) Reduced graphene oxide/CdS for efficiently photocatalystic degradation of methylene blue. J Alloys Compd 524:5–12. doi:10.1016/j.jallcom.2012.02.058

Yang X, Liu J, Yang H, Yu X, Guo Y, Zhou Y, Liu J (2009) Synthesis and characterization of new red phosphors for white LED applications. J Mater Chem 19:3771–3774. doi:10.1039/B819499H

Yang Y, Ma Z, Xu L, Wang H, Fu N (2016a) Preparation of reduced graphene oxide/meso-TiO2/AuNPs ternary composites and their visible-light-induced photocatalytic degradation n of methylene blue. Appl Surf Sci 369:576–583. doi:10.1016/j.apsusc.2016.02.078

Yang Y, Xu L, Wang H, Wang W, Zhang L (2016b) TiO2/graphene porous composite and its photocatalytic degradation of methylene blue. Mater Des 108:632–639. doi:10.1016/j.matdes.2016.06.104

Yin Y, Gan Z, Sun Y, Zhou B, Zhang X, Zhang D, Gao P (2010) Controlled synthesis and photoluminescence properties of BaXO4 (X = W, Mo) hierarchical nanostructures via a facile solution route. Mater Lett 64:789–792. doi:10.1016/j.matlet.2010.01.024

Zhang C, Shen E, Wang E, Kang Z, Gao L, Hu C, Xu L (2006) One-step solvothermal synthesis of high ordered BaWO4 and BaMoO4 nanostructures. Mater Chem Phys 96:240–243. doi:10.1016/j.matchemphys.2005.06.061

Zhang L, Dai J-S, Lian L, Liu Y (2013) Dumbbell-like BaWO4 microstructures: surfactant-free hydrothermal synthesis, growth mechanism and photoluminescence property. Superlattice Microst 54:87–95. doi:10.1016/j.spmi.2012.11.010

Zhang G et al (2017) Facile synthesis of bird's nest-like TiO2 microstructure with exposed (001) facets for photocatalytic degradation of methylene blue. Appl Surf Sci 391(Part B):228–235. doi:10.1016/j.apsusc.2016.04.095

Zhou B, Zhao X, Liu H, Qu J, Huang CP (2010) Visible-light sensitive cobalt-doped BiVO4 (Co-BiVO4) photocatalytic composites for the degradation of methylene blue dye in dilute aqueous solutions. Appl Catal B Environ 99:214–221. doi:10.1016/j.apcatb.2010.06.022

Zhu T, Chen JS, Lou XW (2012) Highly efficient removal of organic dyes from waste water using hierarchical nio spheres with high surface area. J Phys Chem C 116:6873–6878. doi:10.1021/jp300224s

Zouzelka R, Kusumawati Y, Remzova M, Rathousky J, Pauporté T (2016) Photocatalytic activity of porous multiwalled carbon nanotube-TiO2 composite layers for pollutant degradation. J Hazard Mater 317:52–59. doi:10.1016/j.jhazmat.2016.05.056